Designing Sequence-Defined Peptoids for Fibrillar Self-Assembly and Silicification

Wenchao Yang[a, b], Yicheng Zhou[a], Biao Jin[a], Xin Qi[c], Bin Cai[a, d], Qiuxiang Yin[b, e], Jim Pfaendtner[a, c], James J. De Yoreo[a, f], Chun-Long Chen[a, c *]

[a]Physical Sciences Division, Pacific Northwest National Laboratory, Richland, WA 99352, United States.

[b]School of Chemical Engineering and Technology, State Key Laboratory of Chemical Engineering, Tianjin University, Tianjin, 300072, China.

[c]Department of Chemical Engineering, University of Washington, Seattle, WA 98195, United States.

[d]School of Chemistry and Chemical Engineering, Shandong University, Shandong 250100, China.

[e]The Co-Innovation Center of Chemistry and Chemical Engineering of Tianjin, Tianjin University, Tianjin 300072, China

[f]Materials Science and Engineering, University of Washington, Seattle, WA 98105, United States.

*Corresponding author:

E-mail address: Chunlong.Chen@pnnl.gov (Chun-Long Chen)

Key words:

Peptoids, near-neutral pH, fibrillar self-assembly, surface modification, dynamic template, silicification

Abstract:

In the biological environment, mineral crystals exquisitely controlled by biomacromolecules often show intricate hierarchical structures and superior mechanical properties. Among these biominerals, spicules, hybrid silica/protein superstructures serving as skeletal elements in demosponges, represent an excellent example for motivating the synthesis of silica materials. Herein, by designing sequence-defined peptoids containing side chains with a strong binding to silica, we demonstrated that self-assembly of these peptoids into fiber structures enabling the mimicking of both biocatalytic and templating functions of silicatein filaments for the formation of silica fibers at near-neutral pH and ambient temperature. We further showed that the presence of amino groups is significant for the nucleation of silica on self-assembled peptoid nanofibers. Molecular dynamics simulation further confirmed that having silica-binding of amino side chains is critical for self-assembled peptoid fibers in triggering silica formation. We demonstrated that tuning inter-peptoid interactions by varying carboxyl and amino side chains significantly influences the assembly kinetics and final morphologies of peptoid assemblies as scaffolds for directing silica mineralization to form silica spheres, fibers, and sheets. The formation of silica shell on peptoid fibers increased the mechanical property of peptoid hydrogel materials by nearly 1000-fold,

highlighting the great potential of using silicification to tune the mechanical property of hydrogel materials for applications including tissue engineering. Since peptoids are highly robust and programmable, we expect that self-assembly of peptoids containing solid-binding side chains into hierarchical materials open new opportunities in the design and synthesis of highly tunable scaffolds that direct the formation of composite nanomaterials.

1. Introduction:

Silica, the most abundant mineral in the Earth's crust, is also widely observed in marine organisms and higher plants, such as spicules in sponges,[1, 2] frustules in diatoms[2] and plant opals in rice plants.[3] These biogenic silica materials with intricate nano- and microarchitectures and outstanding mechanical properties are formed under the exquisite control of biomacromolecules and mild physiological conditions. In contrast to the harsh reaction conditions (organic solvents, high temperature and additional base or acid) of conventional sol-gel approaches,[4] biocompatible ambient conditions and energy-efficient manners of biosilicification inspired the exploration of biomimetic approaches to synthesize silica-based materials with potential in biomedical and biotechnological applications, such as biosensing,[5] drug delivery[2, 5] and bone regenerations.[2, 6]

Among all the biogenetic silica materials, spicules, needle-like skeletal elements in demosponges, set representative examples of bio-inspired syntheses of silica nanomaterials. They are formed by polycondensation of amorphous silica on highly ordered axial filaments assembled from silicateins (for silica proteins). At neutral pH, the silicatein filaments show dual functions as an efficient biocatalyst and template for triggering silicification.[7] Inspired by these natural processes, many biomimetic approaches have been developed to mimic the *in vivo* functions of silicateins by using synthetic macromolecules.[4, 5] However, translating the extracted underlying principles guiding this bio-triggered silicification to design and synthesize sequence-defined synthetic polymers that promote formation of silica nanominerals remains a significant challenge.[2, 4, 5, 8-13]

Peptoids, namely poly-N-substituted glycines, are a class of sequence-defined synthetic molecules that mimic peptides and proteins.[14-16] Compared with peptides, they have reduced structural complexity owing to their lack of backbone hydrogen bond donors and chirality, enabling us to tune their properties exclusively through side-chain variations.[15, 17] Additionally, the N-substitution also endows peptoids with high stability in most conditions where peptides and proteins cannot function, such as proteolysis[18, 19] and high-temperature[20] conditions. Thanks to these unique advantages, peptoids have been often used for morphological and kinetic controls over the formation of a wide range of inorganic crystals.[17, 21, 22] A large number of amphiphilic peptoids have been synthesized and used as building blocks to assemble into various nanomaterials,[14-16] such as nanosheets,[23-25] nanoribbons,[26, 27] nanotubes[28, 29] and nanofibers,[30, 31] which provide a promising platform for incorporating specific functional groups, including solid-binding residues,[32] into their surfaces of nanomaterials.[17] Taken together, peptoids offer great potential to mimic the biocatalytic and templating functioans of silicatein filaments to promote silica formation.

In this study, by designing sequence-defined peptoids containing side chains with a strong binding to silica, we demonstrated that self-assembly of these peptoids into fiber structures enabling the mimicking of both biocatalytic and templating functions of silicatein filaments to form of silica fibers at near-neutral pH

and ambient temperature. A series of peptoid nanofibers with tunable surface chemistry were synthesized and used for templating silica formation, in which the hydrophobic domain of peptoids controls the fiber structure formation. In contrast, the hydrophilic domain has a significant impact on the fiber formation kinetics and the ability to induce silica formation. By varying the number and arrangement of carboxyl and amino groups in the hydrophilic domain, we obtained one peptoid sequence that exhibits a high efficiency in fiber formation at near-neutral pH and in inducing mineralization to form silica nanofibers. Molecular dynamics (MD) simulations and silica formation results showed that the strong binding of amino groups of self-assembled peptoids to silica is critical in triggering SiO_2 nucleation and growth. We further showed that the formation of silica shell on peptoid fibers enhances the mechanical properties of the peptoid gel networks by nearly 1000-fold, highlighting the great potential of exploiting mineralized peptoid materials as tunable scaffolds for biomedical applications.

2. Materials and Methods

2.1 Materials

β-Alanine t-butyl ester hydrochloride was purchased from Chem-Impex International, Inc. The hydrochloride salt was deprotected by a sodium hydroxide aqueous solution, then extracted with CH2Cl2, filtered, and evaporated under vacuum for further use. Rink amide resin (0.7 to 0.9 mmol/g and 70 to 90 mesh), N,N'-diisopropylcarbodiimide (DIC), bromoacetic acid, and trifluoroacetic acid (TFA) were purchased from Chem-Impex International, Inc and used as received. Tert-Butyl N-(2-aminoethyl)carbamate was purchased from CNH Technologies, Inc and used as received. All other amine submonomers and other reagents are obtained from commercial sources and used without further purification. 0.2M 4-(2-hydroxyethyl)-1-piperazineethanesulfonic acid (HEPES) buffer was made by directly diluting 1.0 M HEPES buffer (pH = 7.3 ± 0.1; Fisher Scientific) with ultrapure water. The ultrapure water was obtained from a Milli-Q water purification system (Millipore Corp., Bedford, MA).

2.2 Peptoid Synthesis

Generally, the peptoid sequences were synthesized using modified solid-phase submonomer synthesis methods as described in the previously published work.[23, 28] The crude products were purified by reverse-phase high performance liquid chromatography (HPLC) on a XBridge Prep C18 10 µm OBDTM (10 µm, 19mm × 100 mm), using adaptable gradient of acetonitrile in H_2O with 0.1% TFA over 15 min. More details of synthesis and purification methods are described in the Supplementary Materials. The purified peptoids were analyzed with ultra performance liquid chromatography (UPLC, Waters, ACQUITY reverse-phase, the corresponding gradient at 0.4 ml/min over 7 min at 40°C with an ACQUITYBEH C18, 17 µm, and 2.1 mm × 50 mm column) that was connected with the mass spectrometry (MS) system (Waters SQD2). The final products were lyophilized and divided into small portions (1.0 or 2.0 µmol) and stored at 4°C.

2.3 Peptoid-Silica Hybrid Material Synthesis

Lyophilized and HPLC-grade peptoids (2.0 µmol) were dissolved in 1 mL of 0.2M HEPES buffer (pH 7.3 ± 0.1). The final concentration of the peptoid stock solution was 2.0 mM. 30 µL of the 2 mM peptoid stock solution with different incubation times was added into 1 mL of 0.2M HEPES buffer (pH 7.3 ± 0.1). 8 µL tetraethyl orthosilicate (TEOS) was added, vortexed for 15 s and then left undisturbed at room temperature for 4 days.

2.4 Characterization

Transmission Electron Microscopy (TEM): TEM samples were prepared by pipetting one drop of solution onto a 3-mm diameter copper grid coated with carbon film. TEM images were taken on the FEI Tecnai G2 transmission electron microscope and JEM 2100 (JEOL) with an accelerating voltage of 200 kV.

Atomic Force Microscopy (AFM): The self-assembled peptoid fibers were characterized by ex situ AFM in air at room temperature using either tapping or ScanAsyst mode with a Bruker MultiMode 8 instrument. The samples were prepared by diluting the self-assembled peptoids with Milli-Q water and using freshly cleaved mica as the substrate.

Scanning Electron Microscopy (SEM): The samples were prepared by pipetting one drop of silicified peptoid solution onto silicon substrates and washed by pipetting Milli-Q water on the silicon substrates and the water was removed by filter paper. SEM measurements were performed on a FEI Helios Nanolab dual-beam focused ion beam of the Helios SEM (FEI Helios NanoLab DualBeam microscope) microscope.

Rheology Studies: The silicified hydrogels were centrifuged at 14000 rpm for 2 min before rheological property measurement. Rheological property study on the samples was performed on a Physica MCR 101 rotational rheometer (Anton Paar USA, Ashland, VA) with a 2.5 cm diameter parallel plate measuring system, PP25/TG coupled with a P-PTD200 Peltier temperature controller. The measuring gap was set at 0.5 mm for all measurements. Samples were measured at room temperature. Measurements were performed for the storage modulus (G'), loss modulus (G"), and complex viscosity (η*) for oscillation frequency ranging from 500 to 0.5 rad/s (79.60 to 0.080 Hz), and strain of 1.6% was applied. Performance check to the rheometer and the measuring system was conducted with a S600 viscosity standard (Cannon Instrument Co. State College, PA USA).

2.5 MD simulations

MD simulations in this study were conducted using GROMACS 5.1[33] with PLUMED 2.6 plugin[34]. The peptoids were described using the CHARMM[35, 36] force field (FF) with modifications on backbone dihedrals following the work by Mirijianian and co-workers[37]. The overall charge states of the Nae and Nce groups were set to be +1 and -1. The silica surface was described using amorphous silica periodic slabs that were terminated with Q3 silanol groups, and 14.3% of the silanol groups were deprotonated to reflect the ionization state at a pH of 7.5.[38] The SPC/E model was used for water molecules and sodium and chloride ions were used to neutralize the charge for Nce6Ahx and Nae6Ahx systems, respectively.

All simulated systems were equilibrated following a minimization, NPT and NVT scheme. The density of the system was adjusted by an NPT equilibration of 0.8 ns with the Bussi-Donadio-Parrinello thermostat[39] and the Berendsen barostat[40] and the configuration was further relaxed for 100 ns with the Bussi-Donadio-Parrinello thermostat. A combination of LINCS[41] algorithm for all h-bonds and a hydrogen mass repartitioning[42] scheme allowed us to use timestep of 4 fs for all simulations.

We used the multiple walkers[43] PBMetaD[44] scheme with dynamically adaptive Gaussians[45] to efficiently calculate the binding affinity between the indicated peptoids and amorphous silica. Five walkers were used for each PBMetaD calculation, and all walkers were initiated with distinct peptoid locations and conformations. The collective variables used in this study included the orthogonal distances between the center of mass (COM) of the peptoid backbone and the silica surface, the orthogonal distances between the COM of each side chain and the silica surface, and the radius of gyration of the peptoid. A total simulation time of 3000 ns (600 ns for each walker) was used to ensure the convergence

of the result. The PLUMED input files required to reproduce the results in this paper are available on PLUMED-NEST (www.plumed-nest.org), the public repository of the PLUMED consortium. The free energy profiles for the COM of the peptoid was obtained through standard reweighting process. The calculations of binding free energy, ΔF_b, follows the protocols in previous work on similar systems.[46, 47]

3. Results and Discussions:

3.1 Peptoid design and synthesis

To select and design peptoid sequences that are suitable for investigating their influences on silica formation, we started with our previously reported peptoid Ncp6Nce6Ahx what was recently reported to form nanofibers through their self-assembly in water[30] and further synthesized two derivatives by changing either half or all Nce group to Nae groups. The peptoids designed in this work are composed of two sub-blocks containing six hydrophobic monomers (N-[2-(4-chlorophenyl)ethyl]glycine, Ncp) and six hydrophilic monomers (N-(2-carboxyethyl)glycine, Nce or N-(2-aminoethyl)glycine, Nae) respectively, with a hydrophobic tail 6-aminohexanoic acid (Ahx) conjugated to their N-terminus as shown in Figure 1. The alternative Nce and Nae groups were chosen because it has been reported that the charge relay effect between neighboring amine and carboxyl acid groups in peptide sequence could endow the peptide with higher catalytic activity towards dehydration of trimethylsilanol than amine alone.[48] Wallace et al. also reported that cooperative interactions between adjacent cationic amino and anionic carboxyl groups on the silica-mineralizing organic templates are significant for triggering silica formation.[49] As for the aromatic residue Ncp, it has been used not only to tune the hydrophobic interactions between peptoids and inorganic particle surfaces,[21, 50, 51] but also to stabilize a variety of self-assembled materials,[23, 24]including nanofibers,[30, 31] by showing enhanced intermolecular interactions, such as π-π interaction.[15, 52] Based on these studies, we reasoned that replacing half or all of the Nce groups with amino-containing Nae groups that exhibit a strong binding to silica[53] would facilitate the self-assembled peptoid materials, including nanofibers, to template the formation of silica nanomaterials,[54] mimicking the biocatalytic and templating functions of silicatein filaments. All these peptoids were synthesized by the solid-phase submonomer synthesis method and purified by HPLC (Figures S1-S3).[28]

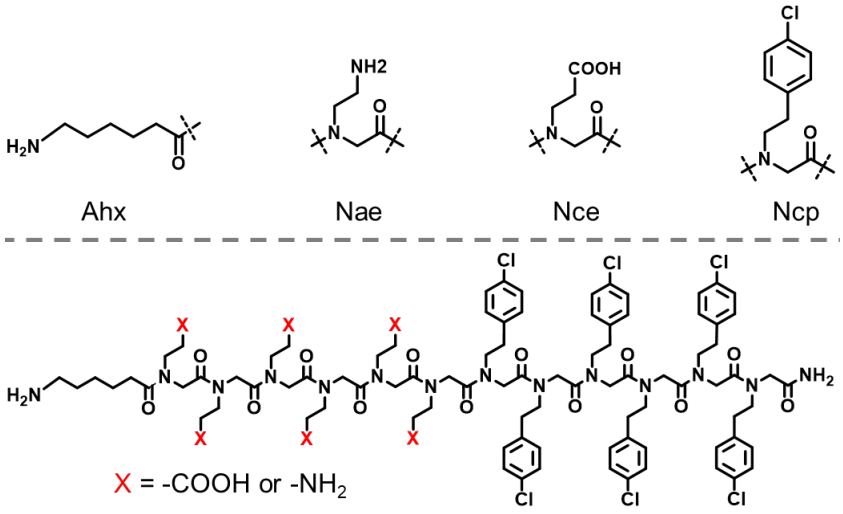

Figure 1. Peptoid side chains and sequences that were used in this work.

3.2 Peptoid self-assembly and silicification.

To synthesize silica nanomaterials, Ncp6Nae6Ahx was first dissolved in HEPES buffer (pH = 7.3 ± 0.1). A clear solution formed at first and gradually became jelly-like (Figure 2a). Rheological measurements of the Ncp6Nae6Ahx solutions were performed to quantify the gelation time. Time-dependent storage modulus G' and loss modulus G'' were recorded at a frequency of 0.5 Hz (Figure 2b). For the freshly-made Ncp6Nae6Ahx solution, both G' and G'' are low at around 0.02 Pa with G'' larger than G', which indicates the viscous nature of the peptoid solution. The G' and G'' begin to increase after about 20-day incubation with G' larger than G'', indicating an elastic solid-like behavior of self-assembled gel-like peptoid materials. AFM results showed that this peptoid hydrogel material formed after 25-day incubation contains many nanofibers (Figure 3b) with a height of ~ 2 nm (Figure S4). TEM results further confirmed the formation of large amount of nanofibers within these hydrogel materials (Figure S5). Based on the proposed structural model of 2D nanosheets assembled from similar peptoids,[23, 24] we conclude that the nanofibers are formed with the six Ncp groups packed in the core along the x-axis through strong hydrophobic interactions, such as π-π interaction, and the hydrophilic domain (Nae6Ahx) displayed on the surface of nanofibers (Figure 3a). It has been reported that the 2D nanosheets formed anisotropically with a faster growth rate along the x-axis than that along the y-axis owing to stronger inter-peptoid interactions along the x direction,[23, 24] which justifies the extension of the nanofibers along the x-axis. After about 45-day incubation, a turbid phase formed and gradually became smaller in size with jellyfish-like morphology at a macroscopic level (Figure 2a). The jellyfish-like sample was further sonicated and analyzed. AFM result showed that this sample contained many nanoribbons (Figure S6a) with a similar height to nanofibers, which indicated lateral growth along the y-axis. Based on the results above, we reason that the self-assembling peptoid solution has two stages: first, the self-assembly of amphiphilic peptoids into nanofibers (Figure 3a); second, the lateral growth of nanofibers to form nanoribbons (Figure S6b). Obtaining peptoid nanofibers that are capable of triggering silification is a key prerequisite for the formation of silica nanofibers.

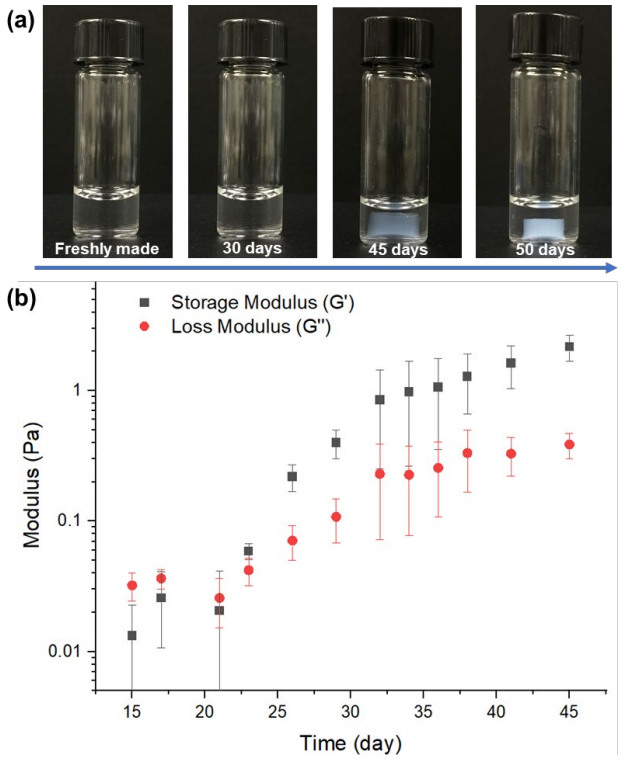

Figure 2. (a) Time-dependent pictures showing the Ncp6Nae6Ahx aqueous solution in HEPES buffer after the corresponding incubation time. (b) Time-dependent storage modulus G' and loss modulus G'' of peptoid assemblies from the Ncp6Nae6Ahx aqueous solution incubated in HEPES buffer.

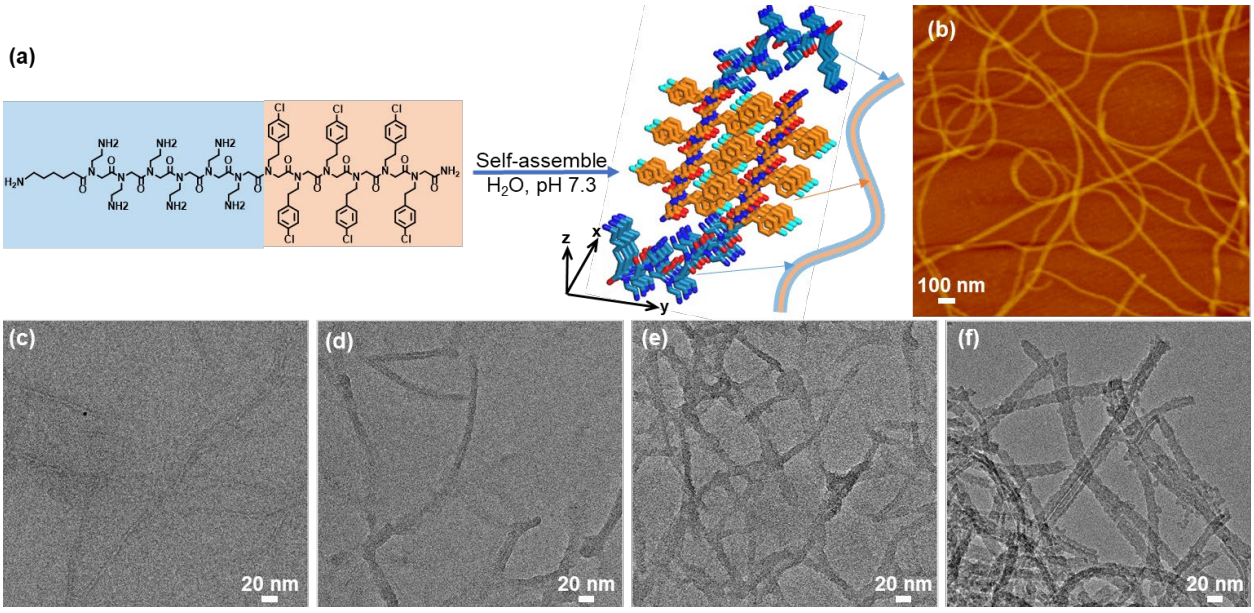

Figure 3. (a) Structure of Ncp6Nae6Ahx and the scheme showing its assembly into nanofibers where N, O and Cl atoms are highlighted in blue, red and cyan colors and the hydrophobic domins are in yellow and hydrophilic domains are in light blue. (b) An AFM image of self-assembled Ncp6Nae6Ahx nanofibers from 25-day incubated peptoid aqueous solution. (c-f) TEM images showing the time-dependent formation of silica fibers induced by Ncp6Nae6Ahx nanofibers. (c) 6.5 h, (d) 8.5 h, (e) 10.5 h and (f) 24 h.

The silica mineralization was initiated by adding TEOS to the aqueous solution containing peptoid nanofibers. The peptoid nanofibers catalyzed the hydrolysis of TEOS and served as templates to form silica nanofibers through the condensation of hydrolyzed TEOS species. Specifically, TEOS was added into the Ncp6Nae6Ahx fibrillar aqueous solutions at pH 7.3 to initiate silica mineralization. Time-dependent TEM results (Figure 3c-f) showed that a uniform silica layer began to deposit on the surface of Ncp6Nae6Ahx fibers at about 6.5 h after TEOS was added. The silica shell thickness gradually increased to ~ 10 nm at 24 h. The axial peptoid nanofibers with low contrast could be easily recognized in the silica fibers (Figure 3f). Under TEM, these silica nanofibers showed typical electron diffraction pattern for amorphous materials and no crystalline electron diffraction pattern could be recognized. Therefore, the silica mineralized on the peptoid nanofibers is amorphous. No silica precipitation occurred under the identical conditions without peptoids, indicating that peptoid fibers serve as highly efficient templates for silicification. To find a suitable window of peptoid assembly to template silica fiber formation, we added TEOS into the Ncp6Nae6Ahx aqueous solutions that were incubated for various number of times (Figure 4). Freshly prepared peptoid solution only induced the formation of uniform silica nanospheres with a diameter of ~ 64 nm (Figures 4e, S7 and S8), which indicated that there were no peptoid fibers in the solution, and the spherical clusters of peptoid assembly with hydrophobic Ncp as cores template silicification to form silica nanosphers. These silica nanospheres were partly fused with each other and flow-induced irregular silica morphologies could be obtained when the silicification occurred with continuous stirring (Figure S8).[55] When peptoid aqueous solution incubated with about 15 days was used for silification, TEM results showed a mixture of silica nanospheres (diameter: 60.2 ± 4.8 nm) and nanofibers (diameter: 52.5 ± 8.0 nm) (Figure 4f), indicating peptoids started to form fiber structures after about 15-day self-assembly. Further increase the incubation time suggested the formation of more and more peptoid nanofibers. As shown in Figure 4g, peptoid assembly solution after 20-day incuation induced the formation of majority of silica nanofibers (Figure 4g). The diameters of formed silica nanofibers decreased to 22 nm when 30-day Ncp6Nae6Ahx solution was used (Figure S7), which could be due to the presence of a further increased number of peptoid fibers serving as templates in the aqueous solution before silification. Interestingly, silica nanoribbons with a height of ~ 20 nm and a diameter ~ 30 nm began to appear when 45-day self-assembled Ncp6Nae6Ahx solution was used as the template for silificiation (Figure S9), this is most likely due to the lateral growth of Ncp6Nae6Ahx nanofibers to form nanoribbons before silicification (Figure S6b). As expected, when 50-day self-assembled Ncp6Nae6Ahx solution was used for silicification, TEM results showed the formation of large amount of silica nanosheets (Figures 4h and S10). We expect that most of peptoid assemblies at this stage present as nanoribbon structures (Figure S6), the silification occurs at both surfaces of nanoribbons, leading to the formation of silica nanosheets. Taken together, 20 to 45-day incubation time of Ncp6Nae6Ahx aqueous solution at pH 7.3 is a suitable window for using this peptoid aqueous solution as the template for the formation of silica fibers; shortening the incubation will lead to the formation of silica nanospheres while an increase incubation time will result in the formation of silica nanosheets due to the formation of peptoid ribbon template.

Additionally, to demonstrate peptoid fibers are stable and could be used under a range of pH conditions for silica fiber formation, we used the Ncp6Nae6Ahx fibers assembled at pH 7.3 to induce silicification at pH 6.2 and 8.9. While peptoid fibers could be observed during the 20 - 40 days incubation for self-assembly, to make sure that there are enough peptoid fibers serving as templates, we used the fiber solution obtained from 34-day self-assembly for silicification experiments. Interestingly, we found that silica fibers were observed in both systems (Figure S11), showing that the assembled Ncp6Nae6Ahx fibers are stable at a wide pH range. The silica fibers formed at pH 8.9 are thinner (diameter: 13.2 ± 2.1 nm) than those

formed at pH 6.2 (diameter: 21.8 ± 0.8 nm), which could be due to the higher binding affinity of protonated Nae groups at pH 6.2 than those at pH 8.9 due to the different degree of positively-charged surfaces of peptoid fibers.

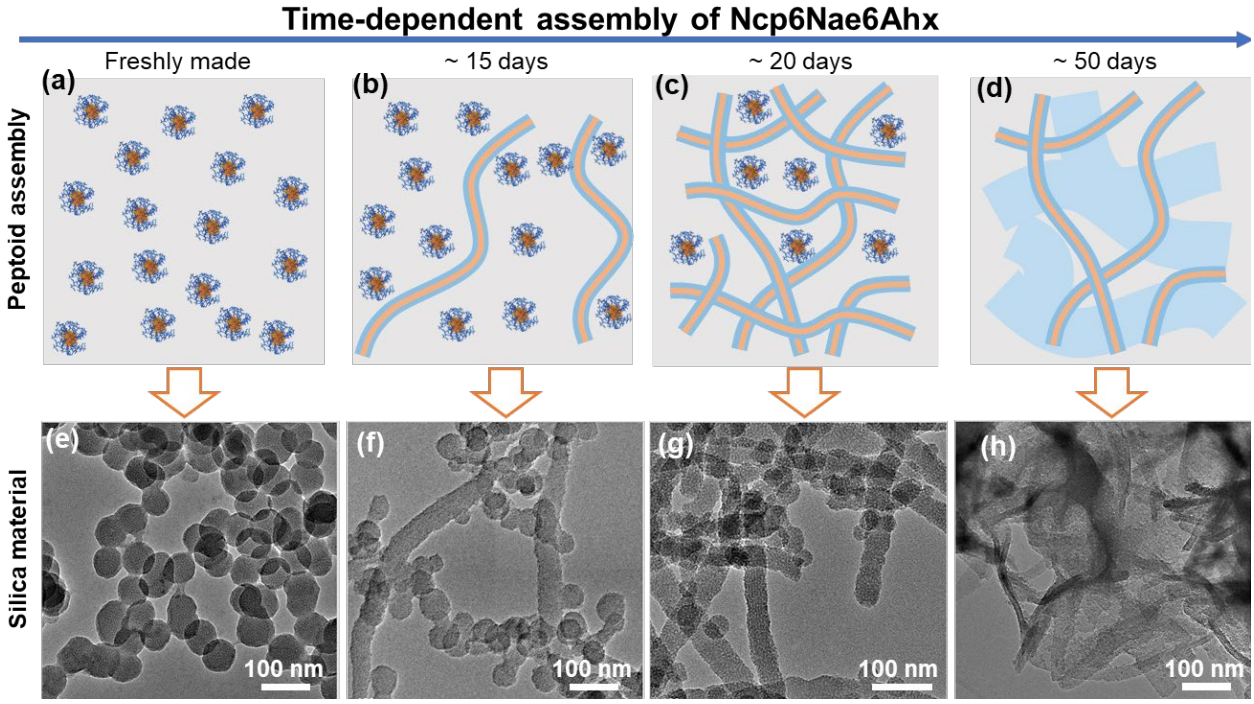

Figure 4. (a-d) Schemes showing the assemblies of Ncp6Nae6Ahx in the aqueous solution at different incubation times. (e-h) TEM images of silica materials templated by the corresponding peptoid assemblies. The blue part represents the hydrophilic surface of self-assembled peptoid structures and the orange part shows the hydrophobic Ncp core.

3.3 Tuning peptoid side chain chemistry for fibrillar self-assembly and silicification.

To further test the role of the peptoid polar domain in the peptoid fibrillar self-assembly and silicification, we synthesized two other peptoids by replacing half or all the Nae groups in Ncp6Nae6Ahx with Nce groups while maintaining the same hydrophobic domain. As for Ncp6(NceNae)3Ahx, time-dependent rheological measurements (Figure 5a) showed a liquid-like behavior (G'' > G') of freshly made Ncp6(NceNae)3Ahx solution at pH 7.3 ± 0.1, which is similar to freshly made Ncp6Nae6Ahx solution. However, the G' and G'' began to increase sharply with G' larger than G'' after about 12-h incubation, which shows a shorter gelation time than that of Ncp6Nae6Ahx solution. As shown in Figure 5b, fiber structures could be easily recognized in one-day Ncp6(NceNae)3Ahx hydrogel (Figure S12), which suggests that the incubation time for the formation of Ncp6(NceNae)3Ahx nanofibers is much shorter than that of Ncp6Nae6Ahx nanofiber. Finally, the hydrogels assembled from Ncp6(NceNae)3Ahx exhibited a nearly 10-fold increase of G' comparing to the Ncp6Nae6Ahx hydrogel, which could be due to the substantive inter-peptoid electrostatic interactions formed between Nce and Nae side-chain groups,[21, 52] while peptoid hydrogels assembled from Ncp6Nae6Ahx lack this type of interactions. Such impact of molecular

interactions on the mechanical stiffness of hydrogels was previously reported in the ABC block copolypeptoid hydrogel systems.[56]

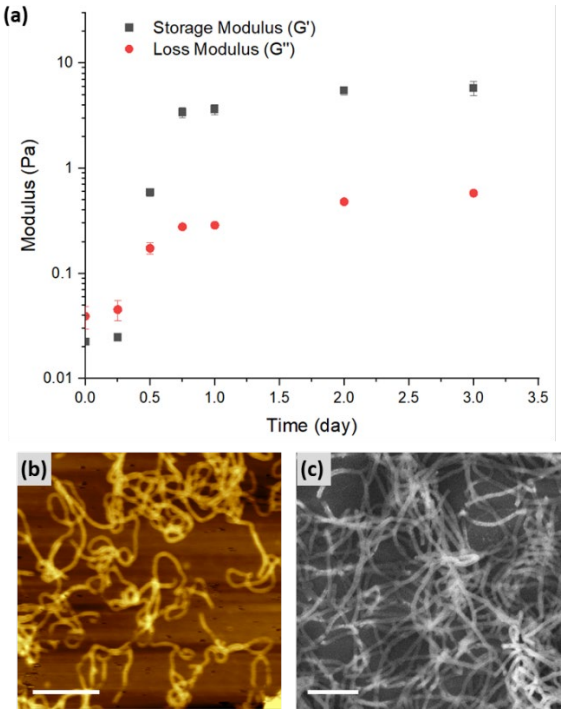

Figure 5. (a) Time-dependent storage modulus G' and loss modulus G'' of Ncp6(NceNae)3Ahx aqueous solution in HEPES buffer. (b) AFM image showing nanofibers self-assembled from Ncp6(NceNae)3Ahx. Scale bar 500 nm. (c) A SEM image showing silica nanofibers induced by freshly made Ncp6(NceNae)3Ahx solution. Scale bar 250 nm.

The Ncp6(NceNae)3Ahx aqueous solutions with different incubation times were then utilized to induce silicification. Uniform silica nanofibers with diameters of 18.2 ± 0.2 nm were obtained by using freshly made Ncp6(NceNae)3Ahx aqueous solution (Figures 5c), indicating this peptoid forms nanofibers much faster than Ncp6Nae6Ahx. The diameters of formed silica nanofibers are slightly smaller than those templated by Ncp6Nae6Ahx nanofibers (Figure S7), which could be due to the reduced positive charges on the peptoid nanofiber surface. It has been reported that the formation of uniform fiber-silica core-shell structures was largely ascribed to the electrostatic attraction between the oppositely charged fiber and silica.[9] In this work, at pH 7.3, Nae and Nce groups were partially ionic with positive and negative charges respectively. Even though half the Nae groups were replaced by Nce groups, the surface of Ncp6(NceNae)3Ahx fibers maintained sufficient positively-charged regions to template the condensation of negatively-charged silica and induced the formation of uniform silica layers. Additionally, we hypothesize that the increased G'' of these peptoid solutions mainly resulted from more and more fibers assembled from peptoid molecules. We unexpectedly observed that increased G'' of Ncp6(NceNae)3Ahx hydrogel did not result in a decrease in the diameters of silica fibers, which was quite different from Ncp6Nae6Ahx system where increased G'' of Ncp6Nae6Ahx solution from 20 to 30 days led to an obvious decrease in diameters of silica fibers (Figure S7). This difference could be interpreted by the fact that Ncp6(NceNae)3Ahx molecules are much more efficient to self-assemble into fiber structures at near-

neutral pH than Ncp6Nae6Ahx molecules. Even though there were no or few fiber structures observed in freshly made Ncp6(NceNae)3Ahx solution, fibrillar self-assembly and Ncp6(NceNae)3Ahx-based silicification could occur simultaneously when TEOS was added into the freshly made peptoid solution. Time-dependent SEM results showed that silica fibers could be easily observed about 7 hours after the addition of TEOS into freshly made Ncp6(NceNae)3Ahx solution (Figure S13), which was comparable to the time it took for Ncp6(NceNae)3Ahx solution to show gel-like behavior (Figure 5a). However, Ncp6Nae6Ahx is not as efficient as Ncp6(NceNae)3Ahx to assemble into fiber structures. Therefore, in contrast to Ncp6(NceNae)3Ahx, Ncp6Nae6Ahx is less likely to form more nanofibers that serve as templates for silica mineralization.

To further demonstrate the importance of polar domain in the fibrillar self-assembly and silicification, peptoid Ncp6Nce6Ahx was synthesized and used for self-assembly and silicification. No self-assembled structures was observed in the Ncp6Nce6Ahx solution at pH 7.3, which could be interpreted by the electrostatic repulsion among ionic Nce groups of peptoids. At pH 6.0, nanofibers could be observed in freshly made Ncp6Nce6Ahx solution where Nce groups become more protonated (Figure S14), which indicated a pH-dependent fibrillar self-assembly enabled by tuning the number and arrangement of Nce and Nae groups [Ncp6(NceNae)3Ahx in Figure 6a] is the best candidate for efficient assembly into fiber structures at near neutral. However, the Ncp6Nce6Ahx solution at pH 6.0 still did not exhibit any gelation trend which could be interpreted by the lack of enough nanofibers in the solution. TEOS was then added into the Ncp6Nce6Ahx solutions at pH 7.3 and 6.0, respectively. No silica precipitation occurred at pH 7.3 and only few irregular silica particles formed at pH 6.0, which indicated that Ncp6Nce6Ahx was almost unable to induce TEOS hydrolysis. Additionally, pre-hydrolyzed TMOS was also used as a silica precursor to evaluate the templating ability of Ncp6Nce6Ahx fibers. Only tiny silica particle networks were obtained in the system where pre-hydrolyzed TMOS was added into the Ncp6Nce6Ahx solution at pH 6.0, which showed that Ncp6Nce6Ahx fibers were unable to template silica condensation (Figure S15). Taken together, it is reasonable to conclude that the peptoid nanofibers with more Nae groups are more efficient as catalytic templates for silicification (Figure 6a).

Next, MD simulations were performed to investigate how peptoid compositions influence the catalytic ability of peptoid assembly to template silicification. We seek to understand the trend in silicification by assessing the binding affinity of the peptoids to silica surfaces at the pH of 7.5. The binding affinity can be compared by using the binding free energy profiles of a single peptoid to an amorphous silica surface (i.e., a suitable representation of silica nanoparticle surface), which can be calculated from MD simulations with parallel-bias metadynamics (PBMetaD).[44] Since the hydrophobic interactions between the Ncp segments drives the formation of fibrils and the polar domains are displayed on the surface to induce silicification, we split the peptoids into characteristic segments as shown in Figure 6a and obtain the binding free energy profiles for each individually (Figure 6b). For the polar domains, our results show a strong binding of Nae6Ahx to silica ($\Delta F_b = 45.9$ kJ/mol), followed by (NceNae)3Ahx ($\Delta F_b = 14.1$ kJ/mol), and non-binding Nce6Ahx. The driving force for binding is likely ascribed to the electrostatic interaction between the positively charged amino groups of Nae side chains and the negatively charged silica surfaces (see Methods). This is lost for negatively charged Nce side chains, which exhibits nearly no affinity to the silica surface. Based on the positive correlation between the binding affinity and the catalytic ability to template silicification, we infer that a strong binding to silica is critical in triggering silica nucleation and growth. This is consistent with previous study showing templates with a stronger binding to crystal

surfaces lead to a faster nucleation rates of corresponding crystals.[54] In addition, the significantly lower binding affinity of Ncp6 to silica ($\Delta F_b = 3.8$ kJ/mol), suggests its inability to promote the precipitation of silica and its major role in templating silicification as the scaffold for the core-shell fibrils.

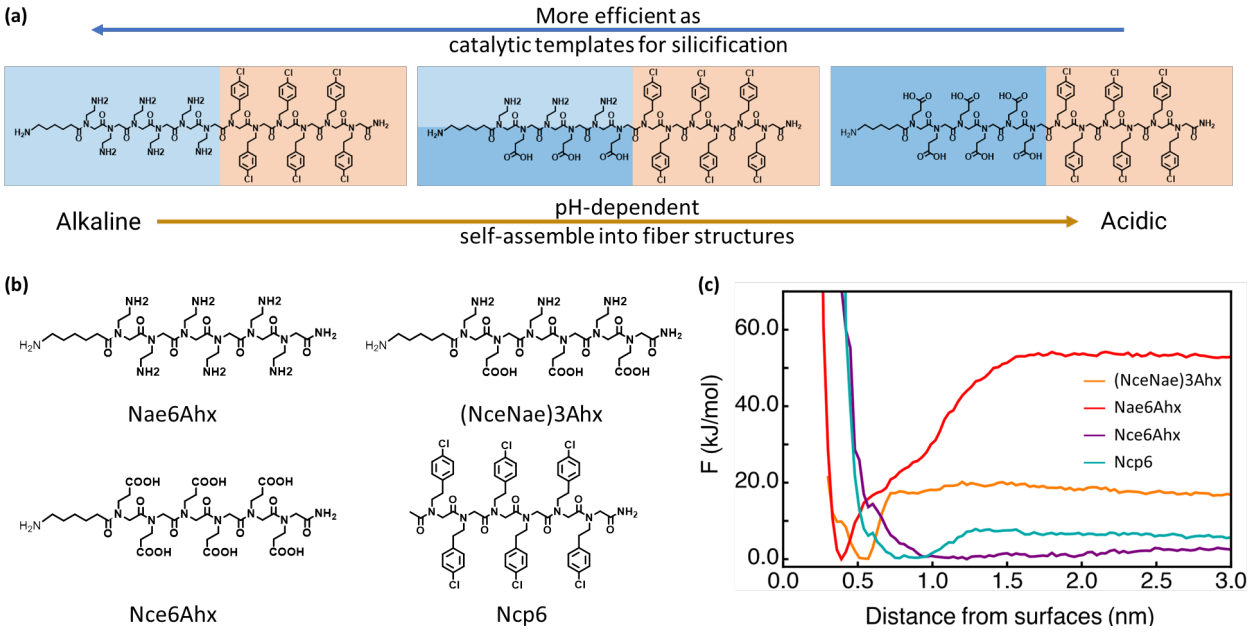

Figure 6. (a) The roles of the peptoid hydrophilic domain in peptoid fibrillar self-assembly and further silicification. (b) Peptoid segments used in the MD simulations. (c) The free-energy profiles of peptoid adsorption on silica surface.

3.4 Mechanical Properties of the Silicified Peptoid Fibrillar Hydrogels

Through biomineralization, minerals can be produced by living organisms to harden or stiffen existing tissues. In this work, we expected that coating the peptoid fibers with a thin layer of silica could improve the mechanical properties of the fibrillar hydrogels with potential application in tissue engineering scaffolds and porous aerogels. Therefore, oscillatory rheology was further performed to evaluate the mechanical properties of the silicified fibrillar hydrogels assembled from Ncp6Nae6Ahx and Ncp6(NceNae)3Ahx. After silicification, all samples were centrifuged for measurement, and dense silicified hydrogels were obtained at the bottom of vials. The liquid was decanted, and the silicified hydrogels were then taken out for rheological property measurement. As for Ncp6Nae6Ahx, the volume fraction of the silicified hydrogels after centrifugation was quite low by using the peptoid solutions with incubation times of no more than 20 days (Figure 7). After 20-day incubation, as much more fibers were formed to serve as templates, the volume fraction of the silicified hydrogels gradually increased to 75% where almost all peptoid molecules assembled in fiber structures. After 36-day incubation, lateral growth of these peptoid nanofibers resulted in the formation of nanoribbon aggregates inducing a sharp decrease in the volume fraction of the silicified hydrogels. Additionally, the formation of silica shell on peptoid fibers could induce nearly 1000-fold enhancement of mechanical properties of peptoid hydrogel materials. While the G' of self-assembled Ncp6Nae6Ahx hydrogel is about 1 Pa, the silicified peptoid hydrogel shows of G' of about

1000 Pa. There was also a similar trend in the mechanical stiffness of the silicified hydrogel as indicated by the G' in Figure 7. There was an increase in the G' owing to more and more fibers serving as templates, followed by a gradual decrease in the G' along with silica morphological changes from fibers, ribbons to nanosheets. Compared with Ncp6Nae6Ahx, there is a rather earlier and narrower window for Ncp6(NceNae)3Ahx to induce the formation of silicified fibrillar hydrogels, which again indicated that Ncp6(NceNae)3Ahx molecules are much more efficient to self-assemble into fiber structures at near-neutral pH. However, the volume fraction of the silicified Ncp6(NceNae)3Ahx hydrogels peaked at 25%, one-third of that of the silicified Ncp6Nae6Ahx hydrogel, which showed that there were still many soluble Ncp6(NceNae)3Ahx molecules that did not assemble into nanofibers to serve as templates. Moreover, the G' of the silicified Ncp6(NceNae)3Ahx hydrogels was only slightly lower than the average G' of the silicified Ncp6Nae6Ahx hydrogels, which could be interpreted by the slight decrease in the thickness of the silica shell around the fiber templates as shown in Figure S7. Taken together, the formation of silica shell could significantly increase the mechanical properties of peptoid hydrogel materials, showing a great potential of exploiting silification to modulate and increase the stiffness of peptoid hydrogel materials for applications including tissue engineering. Given a variety of solid-binding side chains could be introduced in the polar domains of self-assembling peptiods, future directions of this research will be focused on the development of peptoid hydrogels with increased mechanical stiffness and further improving their mechanical properties through peptoid-templated mineralization,[17] such as peptoid-triggered the mineralization of SiO_2, hydroxyapatite[57] and metal carbonates,[50, 51] for the development of functional composite materials.

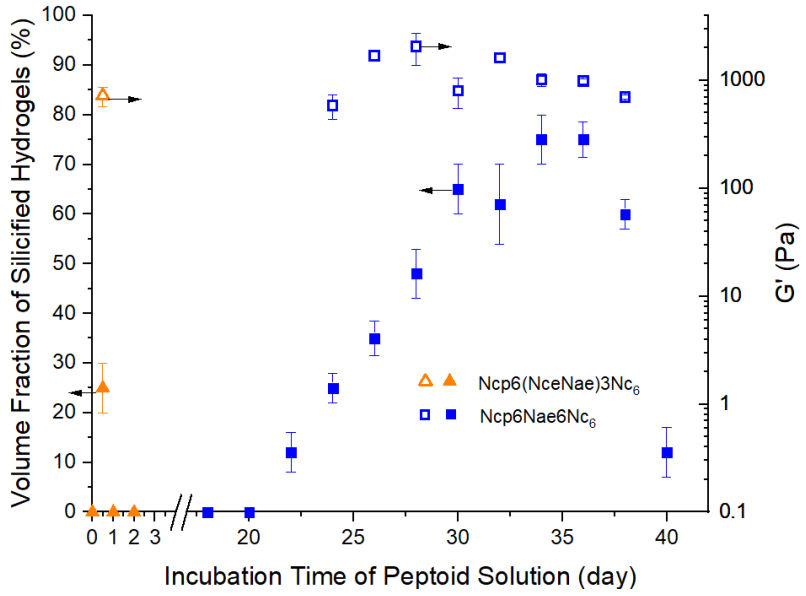

Figure 7. The volume fraction and G' of silica gel after centrifugation.

4. Conclusions:

By including amino- side chains that exhibit a strong binding to silica, we designed and synthesized amphiphilic peptoids that self-assemble into nanofibers as programmable scaffolds for promoting silica formation at near neutral pH, mimicking both the biocatalytic and templating functions of silicatein filaments. These peptoids have the same hydrophobic domains which determine the fiber structure formation, but exhibit tunable hydrophilic domains that significantly influence assembly kinetics and final morphologies of peptoid assemblies. We demonstrated that tuning inter-peptoid interactions by varying the numbers of carboxyl and amino side chains enabled the synthesis of silica spheres, fibers, and sheets. Our results showed that having strong silica-binding domains in the self-assembled peptoids is crucial in triggering silica formation. We further showed that silicification of peptoid fibers significantly improves the mechanical properties of the peptoid hydrogel materials. Because peptoids are sequence-defined, easy to synthesize, and a large amount of solid-binding functional objects[17, 32, 58, 59] could be covalently attached with self-assembling peptoids to form hierarchical materials, we expect that controlled self-assembly of peptoids into hierarchical nanomaterials, including nanofibers, offers a new platform of designing and synthesizing hierarchically structured inorganic nanomaterials, by programming the inter-peptoid and peptoid-particle interactions.

Declaration of Competing Interest

The authors declare that they have no known competing financial interests or personal relationships that could have appeared to influence the work reported in this paper.

Acknowledgments:

This work was supported by the US Department of Energy, Office of Science, Office of Basic Energy Sciences, as part of the Energy Frontier Research Centers program: CSSAS-The Center for the Science of Synthesis Across Scales under Award Number DE-SC0019288. Pacific Northwest National Laboratory (PNNL) is a multi-program national laboratory operated for the Department of Energy by Battelle under contract number DE-AC05-76RL01830. W.Y. acknowledges funding from the China Scholarship Council (CSC).

Appendix A. Supplementary material

Supplementary data associated with this article can be found, in the online version.

References:

[1] R.L. Brutchey, D.E. Morse, Silicatein and the Translation of its Molecular Mechanism of Biosilicification into Low Temperature Nanomaterial Synthesis, Chemical Reviews 108(11) (2008) 4915-4934.
[2] M.A.A. Abdelhamid, S.P. Pack, Biomimetic and bioinspired silicifications: Recent advances for biomaterial design and applications, Acta Biomaterialia 120 (2021) 38-56.
[3] E. Nakamura, N. Ozaki, Y. Oaki, H. Imai, Cellulose intrafibrillar mineralization of biological silica in a rice plant, Scientific Reports 11(1) (2021) 7886.

[4] R.-H. Jin, D.-D. Yao, R. Levi, Biomimetic Synthesis of Shaped and Chiral Silica Entities Templated by Organic Objective Materials, Chem. Eur. J. 20(24) (2014) 7196-7214.
[5] M.J. Limo, A. Sola-Rabada, E. Boix, V. Thota, Z.C. Westcott, V. Puddu, C.C. Perry, Interactions between Metal Oxides and Biomolecules: from Fundamental Understanding to Applications, Chemical Reviews 118(22) (2018) 11118-11193.
[6] Y.K. Jo, B.-H. Choi, C.S. Kim, H.J. Cha, Diatom-Inspired Silica Nanostructure Coatings with Controllable Microroughness Using an Engineered Mussel Protein Glue to Accelerate Bone Growth on Titanium-Based Implants, Adv. Mater. 29(46) (2017) 1704906.
[7] J.N. Cha, K. Shimizu, Y. Zhou, S.C. Christiansen, B.F. Chmelka, G.D. Stucky, D.E. Morse, Silicatein filaments and subunits from a marine sponge direct the polymerization of silica and silicones in vitro, Proc. Natl. Acad. Sci. U. S. A. 96(2) (1999) 361-5.
[8] S. Görlich, A.J. Samuel, R.J. Best, R. Seidel, J. Vacelet, F.K. Leonarski, T. Tomizaki, B. Rellinghaus, D. Pohl, I. Zlotnikov, Natural hybrid silica/protein superstructure at atomic resolution, Proceedings of the National Academy of Sciences 117(49) (2020) 31088.
[9] Y. Cao, S. Bolisetty, G. Wolfisberg, J. Adamcik, R. Mezzenga, Amyloid fibril-directed synthesis of silica core–shell nanofilaments, gels, and aerogels, Proceedings of the National Academy of Sciences 116(10) (2019) 4012.
[10] B. Liu, Y. Cao, Z. Huang, Y. Duan, S. Che, Silica Biomineralization via the Self-Assembly of Helical Biomolecules, Adv. Mater. 27(3) (2015) 479-497.
[11] E.D.E.R. Hyde, A. Seyfaee, F. Neville, R. Moreno-Atanasio, Colloidal Silica Particle Synthesis and Future Industrial Manufacturing Pathways: A Review, Ind. Eng. Chem. Res. 55(33) (2016) 8891-8913.
[12] N. Poulsen, M. Sumper, N. Kröger, Biosilica formation in diatoms: Characterization of native silaffin-2 and its role in silica morphogenesis, Proc. Natl. Acad. Sci. U. S. A. 100(21) (2003) 12075-12080.
[13] N. Kröger, S. Lorenz, E. Brunner, M. Sumper, Self-Assembly of Highly Phosphorylated Silaffins and Their Function in Biosilica Morphogenesis, Science 298(5593) (2002) 584-586.
[14] Z. Li, B. Cai, W. Yang, C.-L. Chen, Hierarchical Nanomaterials Assembled from Peptoids and Other Sequence-Defined Synthetic Polymers, Chem. Rev. 121(22) (2021) 14031-14087.
[15] B. Cai, Z. Li, C.-L. Chen, Programming Amphiphilic Peptoid Oligomers for Hierarchical Assembly and Inorganic Crystallization, Acc. Chem. Res. 54(1) (2021) 81-91.
[16] J. Sun, R.N. Zuckermann, Peptoid polymers: a highly designable bioinspired material, ACS Nano 7(6) (2013) 4715-4732.
[17] W. Yang, Q. Yin, C.-L. Chen, Designing Sequence-Defined Peptoids for Biomimetic Control over Inorganic Crystallization, Chem. Mater. 33(9) (2021) 3047-3065.
[18] S.M. Miller, R.J. Simon, S. Ng, R.N. Zuckermann, J.M. Kerr, W.H. Moos, Proteolytic studies of homologous peptide and N-substituted glycine peptoid oligomers, Bioorg. Med. Chem. Lett. 4(22) (1994) 2657-2662.
[19] S.M. Miller, R.J. Simon, S. Ng, R.N. Zuckermann, J.M. Kerr, W.H. Moos, Comparison of the proteolytic susceptibilities of homologous L-amino acid, D-amino acid, and N-substituted glycine peptide and peptoid oligomers, Drug Dev. Res. 35(1) (1995) 20-32.
[20] R. Li, A. Smolyakova, G. Maayan, J.D. Rimer, Designed Peptoids as Tunable Modifiers of Zeolite Crystallization, Chem. Mater. 29(21) (2017) 9536-9546.
[21] F. Yan, L. Liu, T.R. Walsh, Y. Gong, P.Z. El-Khoury, Y. Zhang, Z. Zhu, J.J. De Yoreo, M.H. Engelhard, X. Zhang, C.-L. Chen, Controlled synthesis of highly-branched plasmonic gold nanoparticles through peptoid engineering, Nat. Commun. 9(1) (2018) 2327.
[22] B. Jin, F. Yan, X. Qi, B. Cai, J. Tao, X. Fu, S. Tan, P. Zhang, J. Pfaendtner, N.Y. Naser, F. Baneyx, X. Zhang, J.J. DeYoreo, C.-L. Chen, Peptoid-Directed Formation of Five-Fold Twinned Au Nanostars through Particle Attachment and Facet Stabilization, Angew. Chem., Int. Ed. 61(14) (2022) e202201980.

[23] H. Jin, F. Jiao, M.D. Daily, Y. Chen, F. Yan, Y.-H. Ding, X. Zhang, E.J. Robertson, M.D. Baer, C.-L. Chen, Highly stable and self-repairing membrane-mimetic 2D nanomaterials assembled from lipid-like peptoids, Nat. Commun. 7(1) (2016) 12252.
[24] F. Jiao, Y. Chen, H. Jin, P. He, C.-L. Chen, J.J. De Yoreo, Self-Repair and Patterning of 2D Membrane-Like Peptoid Materials, Adv. Funct. Mater. 26(48) (2016) 8960-8967.
[25] E.J. Robertson, G.K. Oliver, M. Qian, C. Proulx, R.N. Zuckermann, G.L. Richmond, Assembly and molecular order of two-dimensional peptoid nanosheets through the oil-water interface, PNAS 111(37) (2014) 13284-13289.
[26] X. Ma, S. Zhang, F. Jiao, C.J. Newcomb, Y. Zhang, A. Prakash, Z. Liao, M.D. Baer, C.J. Mundy, J. Pfaendtner, A. Noy, C.-L. Chen, J.J. De Yoreo, Tuning crystallization pathways through sequence engineering of biomimetic polymers, Nat. Mater. 16 (2017) 767-775.
[27] C.L. Chen, R.N. Zuckermann, J.J. DeYoreo, Surface-Directed Assembly of Sequence Defined Synthetic Polymers into Networks of Hexagonally Patterned Nanoribbons with Controlled Functionalities, ACS Nano 10(5) (2016) 5314-5320.
[28] H. Jin, Y.-H. Ding, M. Wang, Y. Song, Z. Liao, C.J. Newcomb, X. Wu, X.-Q. Tang, Z. Li, Y. Lin, F. Yan, T. Jian, P. Mu, C.-L. Chen, Designable and dynamic single-walled stiff nanotubes assembled from sequence-defined peptoids, Nat. Commun. 9(1) (2018) 270.
[29] J. Sun, X. Jiang, R. Lund, K.H. Downing, N.P. Balsara, R.N. Zuckermann, Self-assembly of crystalline nanotubes from monodisperse amphiphilic diblock copolypeptoid tiles, PNAS 113(15) (2016) 3954-3959.
[30] N.A. Merrill, F. Yan, H.B. Jin, P. Mu, C.L. Chen, M.R. Knecht, Tunable assembly of biomimetic peptoids as templates to control nanostructure catalytic activity, Nanoscale 10(26) (2018) 12445-12452.
[31] H. Jin, T. Jian, Y.-H. Ding, Y. Chen, P. Mu, L. Wang, C.-L. Chen, Solid-phase synthesis of three-armed star-shaped peptoids and their hierarchical self-assembly, Biopolymers 110(4) (2019) e23258.
[32] J. Ma, B. Cai, S. Zhang, T. Jian, J.J. De Yoreo, C.-L. Chen, F. Baneyx, Nanoparticle-Mediated Assembly of Peptoid Nanosheets Functionalized with Solid-Binding Proteins: Designing Heterostructures for Hierarchy, Nano Lett. 21(4) (2021) 1636-1642.
[33] M.J. Abraham, T. Murtola, R. Schulz, S. Páll, J.C. Smith, B. Hess, E. Lindahl, GROMACS: High performance molecular simulations through multi-level parallelism from laptops to supercomputers, SoftwareX 1-2 (2015) 19-25.
[34] G.A. Tribello, M. Bonomi, D. Branduardi, C. Camilloni, G. Bussi, PLUMED 2: New feathers for an old bird, Comput. Phys. Commun. 185(2) (2014) 604-613.
[35] K. Vanommeslaeghe, E. Hatcher, C. Acharya, S. Kundu, S. Zhong, J. Shim, E. Darian, O. Guvench, P. Lopes, I. Vorobyov, A.D. Mackerell Jr, CHARMM general force field: A force field for drug-like molecules compatible with the CHARMM all-atom additive biological force fields, J. Comput. Chem. 31(4) (2010) 671-690.
[36] J. Huang, A.D. MacKerell Jr, CHARMM36 all-atom additive protein force field: Validation based on comparison to NMR data, J. Comput. Chem. 34(25) (2013) 2135-2145.
[37] D.T. Mirijanian, R.V. Mannige, R.N. Zuckermann, S. Whitelam, Development and use of an atomistic CHARMM-based forcefield for peptoid simulation, J. Comput. Chem. 35(5) (2014) 360-370.
[38] F.S. Emami, V. Puddu, R.J. Berry, V. Varshney, S.V. Patwardhan, C.C. Perry, H. Heinz, Force Field and a Surface Model Database for Silica to Simulate Interfacial Properties in Atomic Resolution, Chem. Mater. 26(8) (2014) 2647-2658.
[39] G. Bussi, D. Donadio, M. Parrinello, Canonical sampling through velocity rescaling, J. Chem. Phys. 126(1) (2007) 014101.
[40] H.J.C. Berendsen, J.P.M. Postma, W.F. van Gunsteren, A. DiNola, J.R. Haak, Molecular dynamics with coupling to an external bath, J. Chem. Phys. 81(8) (1984) 3684-3690.
[41] B. Hess, H. Bekker, H.J.C. Berendsen, J.G.E.M. Fraaije, LINCS: A linear constraint solver for molecular simulations, J. Comput. Chem. 18(12) (1997) 1463-1472.

[42] C.W. Hopkins, S. Le Grand, R.C. Walker, A.E. Roitberg, Long-Time-Step Molecular Dynamics through Hydrogen Mass Repartitioning, J. Chem. Theory Comput. 11(4) (2015) 1864-1874.
[43] P. Raiteri, A. Laio, F.L. Gervasio, C. Micheletti, M. Parrinello, Efficient Reconstruction of Complex Free Energy Landscapes by Multiple Walkers Metadynamics, J. Phys. Chem. B 110(8) (2006) 3533-3539.
[44] J. Pfaendtner, M. Bonomi, Efficient Sampling of High-Dimensional Free-Energy Landscapes with Parallel Bias Metadynamics, J. Chem. Theory Comput. 11(11) (2015) 5062-5067.
[45] D. Branduardi, G. Bussi, M. Parrinello, Metadynamics with Adaptive Gaussians, J. Chem. Theory Comput. 8(7) (2012) 2247-2254.
[46] X. Qi, Y. Zhao, K. Lachowski, J. Boese, Y. Cai, O. Dollar, B. Hellner, L. Pozzo, J. Pfaendtner, J. Chun, F. Baneyx, C.J. Mundy, Predictive Theoretical Framework for Dynamic Control of Bioinspired Hybrid Nanoparticle Self-Assembly, ACS Nano 16(2) (2022) 1919-1928.
[47] C.M. Mao, J. Sampath, K.G. Sprenger, G. Drobny, J. Pfaendtner, Molecular Driving Forces in Peptide Adsorption to Metal Oxide Surfaces, Langmuir 35(17) (2019) 5911-5920.
[48] T. Kuno, T. Nonoyama, K. Hirao, K. Kato, Influence of the Charge Relay Effect on the Silanol Condensation Reaction as a Model for Silica Biomineralization, Langmuir 27(21) (2011) 13154-13158.
[49] A.F. Wallace, J.J. DeYoreo, P.M. Dove, Kinetics of Silica Nucleation on Carboxyl- and Amine-Terminated Surfaces: Insights for Biomineralization, J. Am. Chem. Soc. 131(14) (2009) 5244-5250.
[50] C.L. Chen, J.H. Qi, R.N. Zuckermann, J.J. DeYoreo, Engineered biomimetic polymers as tunable agents for controlling CaCO3 mineralization, J. Am. Chem. Soc. 133(14) (2011) 5214-5217.
[51] C.L. Chen, J.H. Qi, J.H. Tao, R.N. Zuckermann, J.J. DeYoreo, Tuning calcite morphology and growth acceleration by a rational design of highly stable protein-mimetics, Sci. Rep. 4 (2014) 6266.
[52] C.L. Chen, A.M. Beatty, Guest inclusion and structural dynamics in 2-D hydrogen-bonded metal-organic frameworks, J. Am. Chem. Soc. 130(51) (2008) 17222-17223.
[53] H. Xu, L.B. Casabianca, Probing driving forces for binding between nanoparticles and amino acids by saturation-transfer difference NMR, Sci. Rep. 10(1) (2020) 12351.
[54] M. Hamm Laura, J. Giuffre Anthony, N. Han, J. Tao, D. Wang, J. De Yoreo James, M. Dove Patricia, Reconciling disparate views of template-directed nucleation through measurement of calcite nucleation kinetics and binding energies, Proceedings of the National Academy of Sciences 111(4) (2014) 1304-1309.
[55] J.R. Magana, B. Gumí-Audenis, R.P. Tas, L. Gascoigne, D.L. Atkins, I.K. Voets, Bioinspired Scaffolding by Supramolecular Amines Allows the Formation of One- and Two-Dimensional Silica Superstructures, Chem. Eur. J. 26(66) (2020) 15330-15336.
[56] S. Xuan, C.-U. Lee, C. Chen, A.B. Doyle, Y. Zhang, L. Guo, V.T. John, D. Hayes, D. Zhang, Thermoreversible and Injectable ABC Polypeptoid Hydrogels: Controlling the Hydrogel Properties through Molecular Design, Chem. Mater. 28(3) (2016) 727-737.
[57] Y.-C. Chien, J. Tao, K. Saeki, A.F. Chin, J.L. Lau, C.-L. Chen, R.N. Zuckermann, S.J. Marshall, G.W. Marshall, J.J. De Yoreo, Using Biomimetic Polymers in Place of Noncollagenous Proteins to Achieve Functional Remineralization of Dentin Tissues, ACS Biomaterials Science & Engineering 3(12) (2017) 3469-3479.
[58] C.L. Chen, N.L. Rosi, Peptide-based methods for the preparation of nanostructured inorganic materials, Angew. Chem., Int. Ed. 49(11) (2010) 1924-1942.
[59] M. Monahan, B. Cai, T. Jian, S. Zhang, G. Zhu, C.-L. Chen, J.J. De Yoreo, B.M. Cossairt, Peptoid-directed assembly of CdSe nanoparticles, Nanoscale 13(2) (2021) 1273-1282.